ACS Photonics

Article

pubs.acs.org/journal/apchd5

Shockley–Queisser Detailed Balance Efficiency Limit for Nanowire Solar Cells

Nicklas Anttu*

Division of Solid State Physics and The Nanometer Structure Consortium (nmC@LU), Lund University, Box 118, S–22100 Lund, Sweden

ABSTRACT: III–V semiconductor nanowire arrays show promise as a platform for next-generation solar cells. However, the theoretical efficiency limit for converting the energy of sunlight into electrical energy in such solar cells is unknown. Here, we calculate through electromagnetic modeling the Shockley–Queisser efficiency limit for an InP nanowire array solar cell. In this analysis, we calculate first from the absorption of sunlight the short-circuit current. Next, we calculate the voltage-dependent emission characteristics of the nanowire array. From these processes, we identify how much current we can extract at a given voltage. Finally, after constructing this current–voltage (IV) curve of the nanowire solar cell, we identify from the maximum power output the maximum efficiency. We compare this efficiency of the nanowire array with the 31.0% efficiency limit of the conventional InP bulk solar cell with an inactive substrate underneath. We consider a nanowire array of 400 nm in period, which shows a high short-circuit current. We optimize both the nanowire length and diameter in our analysis. For example, nanowires of 4 μm in length and 170 nm in diameter produce 96% of the short-circuit current obtainable in the perfectly absorbing InP bulk cell. However, the nanowire solar cell emits fewer photons than the bulk cell at thermal equilibrium, especially into the substrate. This weaker emission allows for a higher open circuit-voltage for the nanowire cell. As an end result, nanowires longer than 4 μm can actually show, despite producing a lower short-circuit current, a higher efficiency limit, of up to 32.5%, than the bulk cell.

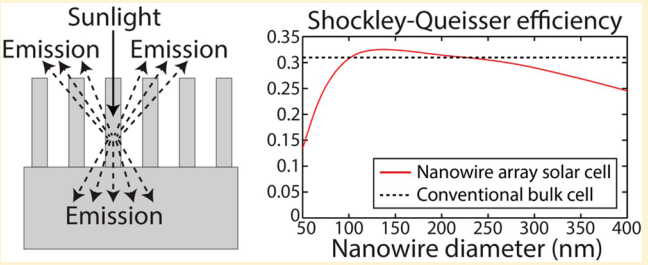

KEYWORDS: *semiconductor, nanowire array, solar cell, Shockley–Queisser efficiency limit*

Both InP[1−3] and GaAs[4,5] nanowire array solar cells have shown very promising performance with a measured highest efficiency of 13.8% when converting the energy in sunlight into electrical energy.[1] Nanowires open up for combining lattice mismatched materials due to strain relaxation in the radial direction.[6] Thus, the nanowire geometry gives a great freedom for the choice of lattice-mismatched materials[6−11] to create heterostructures in the active region of a solar cell. In addition, the expensive III–V material can be fabricated epitaxially in nanowire form on a cheaper but lattice-mismatched substrate.[11,12]

Furthermore, the nanophotonic properties of nanowire arrays can be used for tuning and designing the absorption of light more distinctively than in bulk-like devices,[13−16] and absorption resonances can show up in the individual nanowires.[17−24] For example, a nanowire array, where the nanowires covered only 10% of the substrate surface, absorbed more than 90% of the incident light.[25] A lot of work has been done to optimize the geometry of III–V nanowire arrays[18,24,26,27] in order to maximize the short-circuit current, which is the current extracted under zero voltage bias on the solar cell. However, the efficiency, which depends on the current–voltage relationship of the solar cell, has not been studied with the Shockley–Queisser detailed balance analysis.

Under the conditions where the power output in a solar cell is maximized, the solar cell is forward biased and emits at the same time a voltage-dependent number of photons like a light-emitting diode.[28,29] This emission of photons is the fundamental process that limits the efficiency of an otherwise perfect solar cell.[28] Therefore, the emission characteristics of the nanowire array due to nanophotonic effects[30] needs to be investigated,[31] especially since it is known that the geometry of the nanowires affects strongly the emission.[32,33]

Here, we combine absorption and emission modeling and calculate the Shockley–Queisser detailed balance efficiency limit for an InP nanowire solar cell. For a given solar cell platform, this analysis gives the upper limit for the efficiency by balancing the number of absorbed photons with the number of emitted photons and the number of extracted charge carriers at a given voltage.[28,31] We compare the nanowire-array solar cell with a perfectly absorbing single-junction bulk photovoltaic cell on an inactive substrate. Our analysis gives for such a bulk cell, as a function of the band gap energy, a maximum conversion efficiency of 0.310 for a band gap energy of E_{bg} = 1.34 eV (which is the bandgap energy of InP).

We consider a nanowire array of 400 nm in period, which is known to show a high short-circuit current.[18,27] We optimize both the nanowire length and diameter in our analysis. For

Received: December 23, 2014
Published: January 30, 2015

DOI: 10.1021/ph5004835
ACS Photonics 2015, 2, 446–453

example, nanowires of 4 μm in length and 170 nm in diameter produce 96% of the short-circuit current obtainable in the perfectly absorbing InP bulk cell. However, the nanowire solar cell emits fewer photons than the bulk cell, especially into the substrate. This weaker emission allows for a higher open circuit-voltage for the nanowire cell. As a result, nanowires longer than 4 μm can actually show a higher efficiency limit than the bulk cell, despite producing a lower short-circuit current.

RESULTS AND DISCUSSION

For a solar cell, the current-density versus voltage curve, that is, the IV curve, is given by[34]

$$j = j_{sc} - j_{rec}(V) \tag{1}$$

where j_{sc} is the short-circuit current density due to absorbed photons and $j_{rec}(V)$ is due to the loss of charge carriers by varying recombination processes for a voltage V over the solar cell. From this IV curve, we can calculate the efficiency η of the solar cell through

$$\eta = \frac{j(V_{max})V_{max}}{P_{inc}} \tag{2}$$

where V_{max} is the voltage that maximizes the output power $j(V)V$ of the solar cell and P_{inc} is the incident solar intensity on the cell. Typically for a solar cell, we are interested in j_{sc} and the open-circuit voltage V_{oc}, which is the voltage V at which $j = 0$.

Thus, to analyze the efficiency of a solar cell, we need to construct the IV curve. To calculate the short-circuit current density, j_{sc}, we assume[28] that each absorbed photon with energy above the band gap energy E_{bg} of the single-junction solar cell gives rise to one electron−hole pair that can contribute to the current:

$$j_{sc} = e\int_0^{\lambda_{bg}} \frac{A_{inc}(\lambda)I_{AM1.5}(\lambda)}{\hbar 2\pi c/\lambda} d\lambda \tag{3}$$

Here, $I_{AM1.5}$ is the 1 sun 1000 W/m^2 direct and circumsolar AM1.5D solar spectrum,[35] A_{inc} the absorptance of normally incident light, $\hbar$ the reduced Planck constant, c the speed of light in vacuum, λ the vacuum wavelength of the light, and $\lambda_{bg} = \hbar 2\pi c/E_{bg}$. Notice that we here assume normally incident light, corresponding to $\theta_{inc} = 0°$, in order to maximize the projected area of the solar cell with respect to the incident light. Light incident at an angle $\theta_{inc} > 0$ leads to a decrease in j_{sc} by the factor $\cos(\theta_{inc})$. The absorption in a nanowire array solar cell, that is, $A(\lambda)$, is typically not strongly dependent on the incidence angle for $\theta_{inc} < 50°$, after which it starts to decrease.[24] Therefore, we expect that normally incident light maximizes the short-circuit current density in the nanowire array solar cell.

The second term in eq 1, j_{rec}, includes the loss of charge carriers due to radiative and nonradiative recombination, as well as for example the Ohmic losses in contacts and inside the solar cell. Previously, electrical drift-diffusion modeling for the transport of electrons and holes in nanowire array solar cells has been performed. In these studies, finite mobility of the electrons and the holes, nonradiative Shockley−Read−Hall recombination, and surface recombination limited the solar cell performance.[36−40]

However, the efficiency limit for a solar cell arises from purely optical considerations. When a solar cell absorbs photons, it must also emit photons due to the reciprocity between absorption and emission of light.[28,31] These emitted photons stem from the radiative recombination of electron−hole pairs. When calculating the upper value for the efficiency limit for a given solar cell platform, we include only this fundamentally required radiative recombination process:[28]

$$j_{rec}(V) = eF_{c0}[\exp(eV/k_bT) - 1] \tag{4}$$

where k_b is the Boltzmann constant. Here, F_{c0} is the number of photons the solar cell emits at thermal equilibrium, that is, at the voltage bias $V = 0$, corresponding to the blackbody emission of the solar cell. Thus, in eq 4, the blackbody emission F_{c0} of the solar cell is enhanced exponentially by the voltage over the solar cell.[31] By combining eqs 1 and 2, we obtain for the solar cell the ideal diode equation $j = j_{sc} - j_0[\exp(eV/k_bT) - 1]$ with $j_0 = eF_{c0}$ the reverse bias saturation current. Note that this j_0 arises from the fundamentally required emission of photons and therefore shows the lowest possible value since all other nonintrinsic loss mechanisms are excluded.[28]

Thus, to construct the IV curve of the solar cell in eq 1 for the efficiency analysis (eq 2), we need to calculate the number of photons emitted at thermal equilibrium, F_{c0}, which depends on the emission characteristics of the solar cell. For this purpose, we use the reciprocity between the absorptance A and the emissivity e_{em}.[31] This reciprocity leads to the detailed balance of $A_{TE}(\lambda,\theta,\varphi) = e_{em,TE}(\lambda,\theta,\varphi)$ and $A_{TM}(\lambda,\theta,\varphi) = e_{em,TM}(\lambda,\theta,\varphi)$.[31] Here, TE and TM denote the transverse electric and the transverse magnetic polarization, respectively.[31] Furthermore, θ and φ are the polar and azimuth angles that determine the propagation direction of the light (Figure 2). In this way, we can calculate the emission rate of photons into the top and the bottom side of the solar cell with real-valued refractive index n_{top} and n_{bot}, respectively:[28,31]

$$F_{c0,top(bot)} = \int_0^{2\pi} d\phi \int_0^{\pi/2} d\theta \int_0^{\lambda_{bg}} d\lambda \frac{cn_{top(bot)}^2}{\lambda^4} \times \frac{A_{TE,top(bot)}(\lambda,\theta,\phi) + A_{TM,top(bot)}(\lambda,\theta,\phi)}{\exp[(\hbar 2\pi c/\lambda)k_BT] - 1} \cos(\theta)\sin(\theta) \tag{5}$$

where $\theta \equiv \theta_{top}$ in the top region and $\theta \equiv \theta_{bot}$ in the bottom substrate region (see Figure 2 for a schematic). Then, $F_{c0} = F_{c0,top} + F_{c0,bot}$.

First, we calculate from eqs 1−5 the efficiency limit of the conventional single-junction planar bulk cell for varying band gap energy to have a reference for comparison with the nanowire solar cell. We consider a perfectly absorbing bulk cell and set $A_{inc}(\lambda) = 1$ to maximize the short-circuit current density in eq 3,[28] and we use $T = 300$ K. Similarly, we assume in eq 5 that $A_{TE,top(bot)}(\lambda,\theta,\varphi) = A_{TM,top(bot)}(\lambda,\theta,\varphi) = 1$ when $\lambda < \lambda_g$.[28,41] We focus on the system shown in the inset in Figure 1 with air on the top ($n_{top} = 1$) and an inactive semiconductor substrate at the bottom, which is a typical configuration for nanowire array solar cells.[1−5] We set the refractive index of the substrate to $n_{bot} = 3.5$ to represent a typical semiconductor substrate (notice that the real part of the refractive index of, for example, InP varies from 3.5 to 3.4 for $850 < \lambda < 925$ nm in which range we expect the emission to occur; see Figure 5). The calculated efficiency for this planar cell as a function of band gap energy (Figure 2) shows a peak of $\eta = 0.310$ at $E_{bg} = 1.34$ eV. Notice that InP has this band gap energy of 1.34 eV that maximizes the efficiency. Therefore, we choose InP for the nanowire material for this study. For this $E_{bg} = 1.34$ eV, the planar bulk cell shows $j_{sc} = j_{sc,planar} = 34.6$ mA/cm^2, which we denote also as $j_{sc,max}$ since this is the maximum value for InP. We find, furthermore, for this bulk cell that $V_{oc} = V_{oc,planar} = 1.01$ V.

DOI: 10.1021/ph5004835
ACS Photonics 2015, 2, 446−453

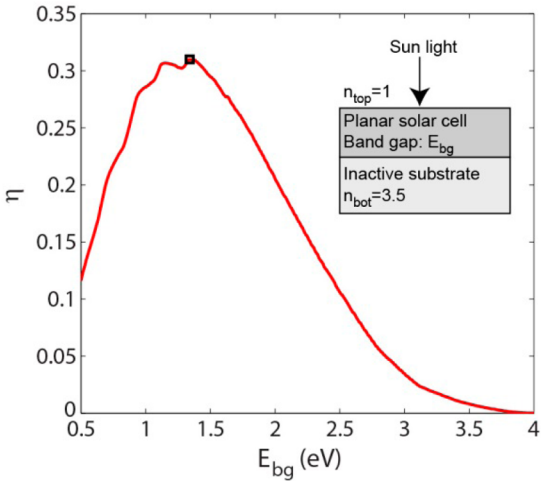

Figure 1. Shockley–Queisser detailed balance efficiency limit, η, for a perfectly absorbing planar bulk cell, shown here for varying band gap energy E_{bg}. The region on top of the cell has refractive index n_{top} = 1 and the substrate underneath the cell has n_{bot} = 3.5 (see the inset for a schematic). The square marks the band gap energy of 1.34 eV, where the efficiency peaks at η = 0.310. Notice that the band gap energy of InP is 1.34 eV.

We choose to fix the period of the nanowire array (Figure 2) to p = 400 nm since this gives a high short-circuit current for $L \approx 1-4$ μm when $D \approx 180$ nm.[18,27] We perform for each D and L electromagnetic modeling to obtain the $A_{TE,top(bot)}(\lambda,\theta,\varphi)$ and $A_{TM,top(bot)}(\lambda,\theta,\varphi)$ needed for the efficiency analysis in eqs 1–5. The modeling is performed with a scattering matrix method,[42] which solves the Maxwell equations for incident light. The optical properties of the nanowire material is taken into account in the modeling through tabulated values for the bulk refractive index n of InP.[43] For the air between and on top of the nanowires we use n_{top} = 1, and for the substrate n_{bot} = 3.5. We perform the modeling for 50 < D < 400 nm in steps of 5 nm and L = 0.5, 1, 2, 4, 8, 16, and 32 μm.

First, we find that for all nanowire lengths and diameters (Figure 3a) the nanowire solar cell shows a lower short-circuit current density than the bulk cell, that is, $j_{sc} < j_{sc,max}$ = 34.6 mA/cm^2. For the shortest nanowire length, we find a maximum j_{sc} of 24.7 mA/cm^2. However, we notice that j_{sc} approaches $j_{sc,max}$ with increasing L, and for L = 32 μm, we find that j_{sc} peaks at 34.2 mA/cm^2. This increasing j_{sc} with L can be understood from an increased absorption in the nanowires with increasing length. Furthermore, the nanowire diameter that maximizes j_{sc} for a given length decreases with increasing nanowire length, from D = 185 nm for L = 2 μm to D = 140 nm for L = 32 μm where j_{sc} = 34.2 mA/cm^2. This decreasing D for the optimized structure can be understood from decreasing reflection losses at the top of the nanowires with decreasing D, where the expected decreasing absorption with decreasing D is compensated by the increasing L.

When regarding the efficiency, we find for the shortest nanowire length L = 0.5 μm a maximum of η = 0.226, considerably lower than the efficiency η_{planar} = 0.310 of the corresponding planar bulk cell. However, for $L \geq 4$ μm, $\eta > \eta_{bulk}$ = 0.310, and for the length L = 32 μm, η seems to saturate toward 0.325 (Figure 3b). Thus, the nanowire solar cell can show a higher efficiency limit than the conventional bulk cell (Figure 3b), despite generating a lower short-circuit current j_{sc} (Figure 3a).

To understand how the nanowire solar cell can show a higher efficiency despite a lower short-circuit current density, we turn to study the voltage characteristics of the solar cell. We find that for all L, $V_{oc} > V_{oc,planar}$ (Figure 3c). In a conventional solar cell, V_{oc} depends on j_{sc} since from eqs 1 and 4, $V_{oc} \approx k_bT \log[j_{sc}/(eF_{c0})]/e$. Therefore, we could, contrary to the behavior found here for the nanowire solar cell versus the bulk cell, expect a lower open-circuit voltage for the nanowire solar cell due to the lower j_{sc}. To explain the larger V_{oc} in the nanowire array, we are left with the option that the nanowire array emits fewer photons at thermal equilibrium. That is, F_{c0} for the nanowire array is lower than for the bulk cell.

We note that, in principle, it is possible to increase the effective (optical) band gap E_{eff} of the solar cell by suppressing the emission close to the band gap region.[44] Such an effect shows up as e_{em} = 0 for $E_{bg} < E < E_{eff}$ (corresponding to $\lambda_{eff} < \lambda < \lambda_{bg}$) in eq 5. Such a decrease in F_{c0} could lead to an increased open-circuit voltage, as seen from $V_{oc} = k_bT \log[j_{sc}/(eF_{c0})]/e$.[44] However, since the E_{bg} = 1.34 eV of InP in this study gives a

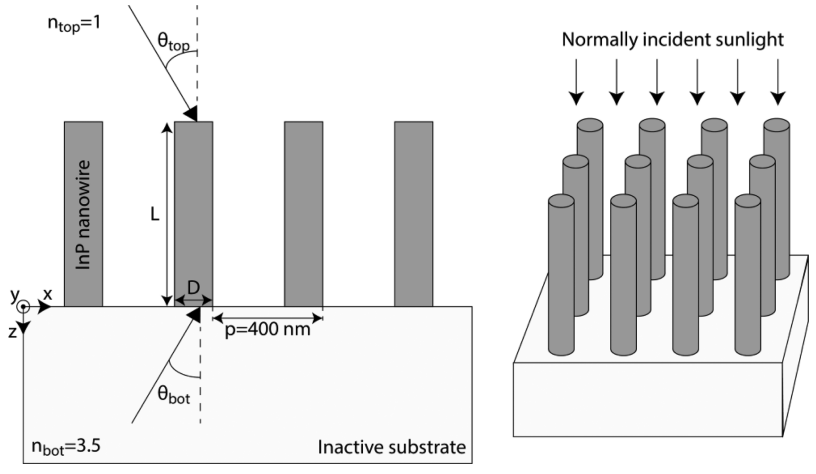

Figure 2. (Left) 2D cross-section of an InP nanowire array. θ_{top} and θ_{bot} denote, respectively, the propagation direction of light in the top region with a refractive index n_{top} = 1 and in the bottom region with a refractive index n_{bot} = 3.5. The nanowires are of diameter D and length L and arranged in a square pattern of period p = 400 nm. Here, the azimuth angle φ = 0 (φ = 90°) indicates light that propagates in the x–z (y–z) plane. (Right) 3D schematic of the nanowire array with sunlight incident at normal angle, that is, from the angle θ_{top} = 0.

DOI: 10.1021/ph5004835
ACS Photonics 2015, 2, 446–453

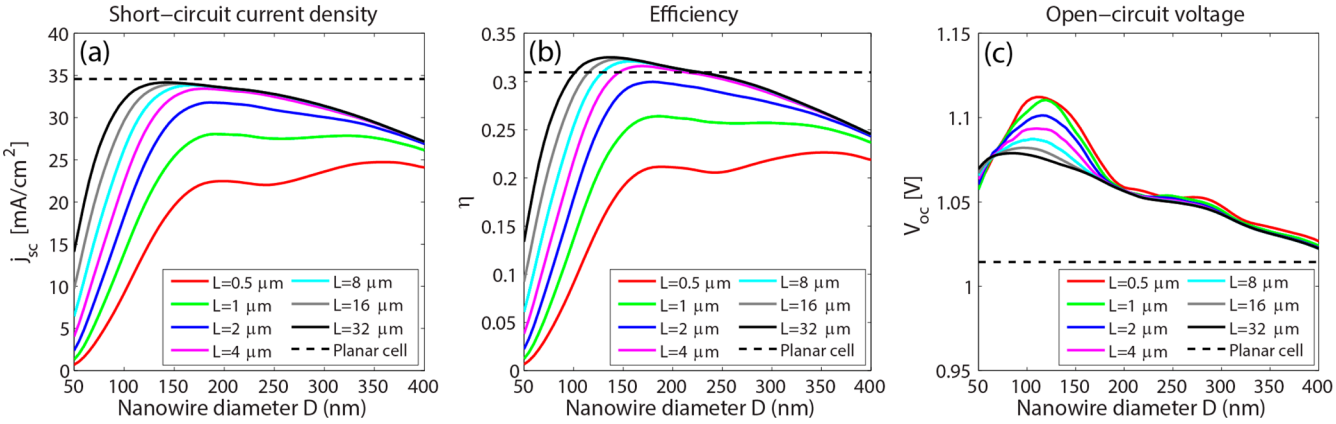

Figure 3. (a) Short-circuit current density j_{sc} of the InP nanowire solar cell for varying nanowire length L and diameter D (see Figure 2 for a schematic). Here, we show with the dashed line also the current density $j_{sc,max}$ = 34.6 mA/cm^2 of the perfectly absorbing planar InP bulk cell (see inset in Figure 1 for a schematic). (b) Same as (a) but for the efficiency η with the efficiency η_{planar} = 0.310 of the planar bulk cell shown by the dashed line. (c) Same as (a) but for the open-circuit voltage V_{oc} together with the $V_{oc,planar}$ = 1.01 V of the planar bulk cell (dashed line). This modeling is performed for the AM1.5 direct and circumsolar 1 sun 1000 W/m^2 spectrum.

maximum efficiency limit obtainable for a single-junction bulk-type solar cell (Figure 1), a simple increase of the effective band gap from 1.34 eV cannot increase the efficiency limit beyond η = 0.310 by increasing the V_{oc}. Such an increase of V_{oc} would decrease j_{sc} more rapidly [notice that e_{em} = 0 for $E_{bg} < E < E_{eff}$ requires a reduction in the absorption of the sunlight, that is, also A_{inc} = 0 for $E_{bg} < E < E_{eff}$ in eq 3], leading to an overall decrease of efficiency since E_{bg} = 1.34 eV is already at the maximum of the efficiency. Thus, we are left with the option that F_{c0} is decreased below that in the conventional bulk cell, increasing V_{oc} without sacrificing j_{sc} in the same proportion.

To study in more detail how we reach in the nanowire arrays values beyond the bulk limit of η = 0.310, we concentrate on L = 4 μm which shows for the optimized D = 170 nm a short-circuit current density of 96% of $j_{sc,max}$ but still a higher η than the bulk cell due to the higher V_{oc}. As discussed above, $V_{oc} = k_bT \log[j_{sc}/(eF_{c0})]/e$ and $j_{sc} < j_{sc,planar}$. In order to understand this higher V_{oc}, we need to look at F_{c0}, which is determined by the emission properties of the solar cell into both the air superstrate and the substrate (eq 5). We show in Figure 4 the contribution to eF_{c0} from emission into the top ($eF_{c0,top}$) and the bottom ($eF_{c0,bot}$) side.

For D < 150 nm, the emission into the n_{top} = 1 air superstrate top region and the n_{bot} = 3.5 substrate bottom region are almost equal. This behavior is in strong contrast to the conventional bulk cell where the emission into the n_{bot} = 3.5 substrate is enhanced by a factor of $n_{bot}^2 = 3.5^2$ = 12.25 as seen both from eq 5 and Figure 4. For D > 150 nm in the nanowire array, the emission into the substrate becomes dominating with increasing D, with 10.5× more photons emitted for D = 400 nm into the n_{bot} = 3.5 substrate compared to into the n_{top} = 1 superstrate.

Next, we concentrate on the system of D = 170 nm, which maximizes η for L = 4 μm (Figure 3b). We show in Figure 5 the emission into the n_{top} = 1 top region and the bottom n_{bot} = 3.5 substrate side as a function of wavelength.[45] As found above for the wavelength-integrated emission (Figure 4), the emission is here very similar to both sides for all wavelengths, even if the higher density of optical states in the n_{bot} = 3.5 substrate could in principle allow for a 3.5^2 = 12.25× higher emission rate. To understand why the emission into the substrate does not reach such high values, we show in Figure 6 the emission pattern as a

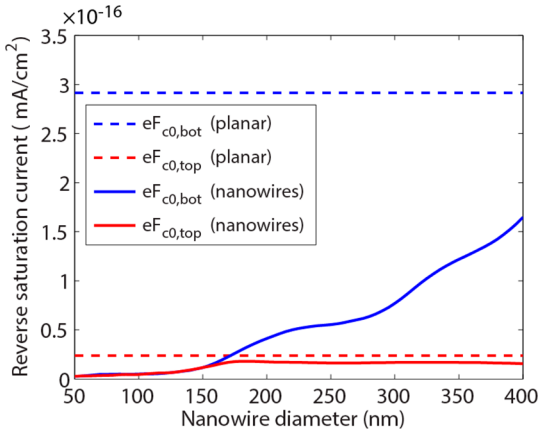

Figure 4. Reverse saturation current density $j_0 = eF_{c0} = eF_{c0,top} + eF_{c0,bot}$ in eq 4, as determined from eq 5 by emission of photons into the n_{top} = 1 top side and the n_{bot} = 3.5 substrate at the bottom, respectively. Here, we show results for an InP nanowire array with L = 4 μm, p = 400 nm, and varying diameter D (see Figure 2 for a schematic) together with the results for the planar bulk cell (see inset in Figure 1 for a schematic).

function of emission angle for λ = 900 nm, which is in the vicinity of the band gap wavelength of 925 nm.

We find that the solar cell emits light in principle into all angles (Figure 6), that is, $e_{em} > 0$ for all θ and φ (see Figure 2 for a schematic of these angles). Note that the sunlight is, in principle, incident from a small solid angle of 6.85 × 10^{-5} sr centered around θ = 0 (corresponding to light incident for θ < 0.27° = θ_{sun}).[28] Due to reciprocity, light must be emitted into these angles if it is absorbed from these angles, which gives a lower limit for F_{c0}. However, the light that is emitted into $\theta > \theta_{sun}$ increases F_{c0} above this lower limit. Therefore, by limiting the emission to $e_{em} < 1$ for angles $\theta > \theta_{sun}$ from which light is not incident, F_{c0} decreases, and consecutively V_{oc} and η can be increased without sacrificing the short-circuit current density j_{sc}.[46]

When we study the angular dependent emission pattern for D = 170 nm, the emission into the n_{top} = 1 top side is not strongly angle dependent (Figure 6a) until we reach close to grazing incidence (θ = 90°) where the emissivity goes to zero due to total internal reflection. In strong contrast, the emissivity

DOI: 10.1021/ph5004835
ACS Photonics 2015, 2, 446−453

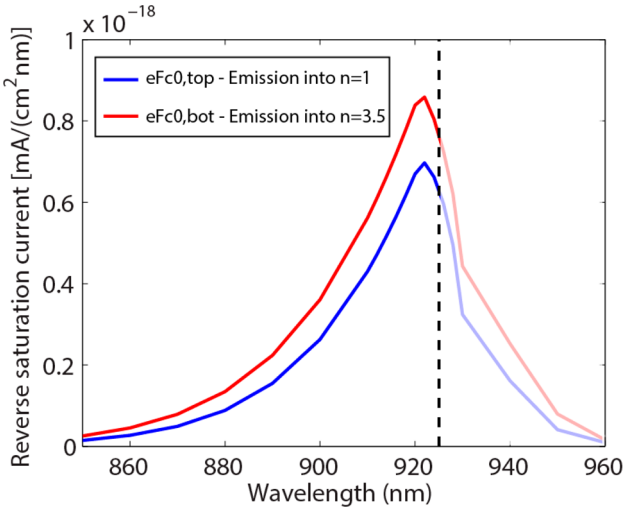

Figure 5. Contribution to the reverse saturation current $j_0 = eF_{c0} = eF_{c0,top} + eF_{c0,bot}$ in eq 4, as determined from eq 5 by emission of photons into the $n_{top} = 1$ top side and the $n_{bot} = 3.5$ substrate at the bottom, respectively, as a function of emission wavelength. Here, we show results for an InP nanowire array with $L = 4$ μm, $p = 400$ nm, and $D = 170$ nm (see Figure 2 for a schematic).

into the $n_{bot} = 3.5$ bottom side (Figure 6b) drops rapidly over the angles $20° < \theta < 30°$ toward values of $e_{em} < 0.05$ for large θ. Thus, there is a process that prohibits efficient emission of light into large angles in the $n_{bot} = 3.5$ substrate. We note that the critical angle for total internal reflection at an interface between a material of refractive index $n = 1.5$ and a material of $n = 3.5$ is given by $\text{asin}(1.5/3.5) = 25.4°$. We do not expect efficient emission from the $n = 1.5$ region into angles beyond the critical angle in the $n = 3.5$ region. Thus, from the drop of the emissivity over $20° < \theta < 30°$, it seems that the nanowire array with $D = 170$ nm behaves for the emission into the $n_{top} = 3.5$ substrate approximately as a material of refractive index close to 1.5, or equivalently, the $n_{top} = 3.5$ substrate looks for the emission like an $n = 1.5$ substrate. In this way, we can use the high-refractive index InP material in nanowire form on top of a high-refractive index substrate without increasing the emission of photons compared to a low-refractive index substrate.

Notice that the optical response of nanowire arrays has been found to be strongly dependent on the HE_{11} waveguide mode of the individual nanowires.[18] Therefore, we calculated the propagation constant β_{HE11} of the HE_{11} mode for an InP nanowire of the 170 nm diameter considered above in Figure 6b. From this propagation constant, we can calculate a refractive index $n_{HE11} = \text{Re}(\beta_{HE11})/(2\pi/\lambda)$ for the mode. We find that n_{HE11} decreases from 1.3 to 1.1 when λ increases from 850 to 925 nm, which is the wavelength range where the emission occurs (see Figure 5). We note that the critical angle for total internal reflection from a bulk region of refractive index $n_{HE11} = 1.2$ to a bulk region of $n_{bot} = 3.5$ is 20.1°. Thus, the drop in the emissivity that starts to occur at $\theta = 20°$ in Figure 6b coincides well with the expectation from the refractive index of the HE_{11} mode.

Next, when we study the case of $D = 400$ nm and emission into the $n_{top} = 1$ top side (Figure 6c), we find values close to

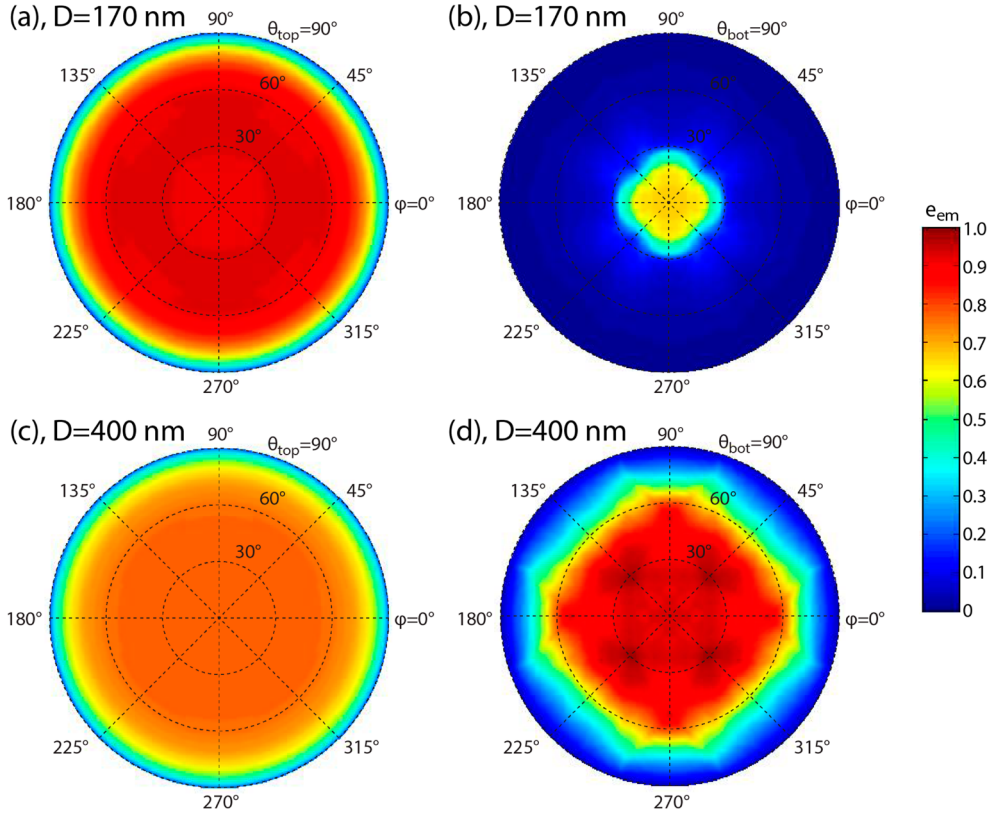

Figure 6. Emissivity e_{em} of a nanowire array with period $p = 400$ nm and nanowires of $L = 4$ μm in length as a function of polar angle θ and azimuth angle φ (see Figure 2 for a schematic). (a, b) Emissivity for nanowires of diameter $D = 170$ into (a) the top $n_{top} = 1$ region and (b) into the bottom $n_{bot} = 3.5$ substrate. (c, d) Same as (a) and (b) but for a nanowire diameter of 400 nm. The results are for $\lambda = 900$ nm and averaged for TE and TM polarization.

DOI: 10.1021/ph5004835
ACS Photonics 2015, 2, 446−453

0.75 for $\theta < 60°$. These values are in good agreement with the emissivity $e_{em} = (1 - R) = 0.701$ into a region of $n = 1$ at normal angle ($\theta = 0$) from a bulk layer of refractive index $n_{InP} = 3.41 + i0.09$, corresponding to the InP at the considered $\lambda = 900$ nm. Here, $R = |n_{InP} - 1|^2/|n_{InP} + 1|^2 = 0.299$ is the reflectance at normal angle. Thus, from this good agreement, we conclude that the nanowire array with $D = 400$ nm, where the nanowires cover $\pi(D/2)^2/p^2 = 79\%$ of the substrate surface, starts to resemble optically a continuous bulk film. Similarly, for the emission into the $n_{bot} = 3.5$ substrate for $D = 400$ nm (Figure 6d), $e_{em} \to 1$ for small θ indicating that light can couple between the nanowire array and the substrate without considerable reflection losses. For $\theta \to 90°$ we find however that $e_{em} \to 0$ due to the remaining refractive index mismatch between the nanowire array and the substrate, which leads to total internal reflection at the grazing angle.

Finally, we comment on the possibility to reach in nanowire array solar cells open-circuit voltages and efficiencies beyond those of a bulk cell also in the case where nonradiative bulk recombination determines j_0. In the case of such nonradiative recombination, the reverse bias saturation current through a unit cell of area $p \times p$ of the nanowire array containing one nanowire of diameter D is given by $I_{0,uc} = \pi(D/2)^2 j_{0,planar}$. Here, $j_{0,planar}$ is the reverse bias saturation current of the planar bulk cell and depends on the density of the nonradiative recombination centers, which is assumed equal to that in the nanowires. In this case, the reverse saturation current density of the nanowire array is given by $j_0 = I_{0,uc}/p^2 = f \times j_{0,planar}$. Here, $f = \pi(D/2)^2/p^2$ is the fraction of the substrate surface covered by nanowires. Thus, due to the reduced cross-sectional area of the nanowires compared to the bulk cell, j_0 is reduced here by the factor f. However, due to light concentration, the nanowires can absorb 100% of the incident light. That is, $A(\lambda) \to 1$ for $\lambda < \lambda_{bg}$ is possible even if the nanowires cover only a fraction f of the surface. Thus, $j_{sc} \to j_{sc,planar}$ is, in principle, possible (see Figure 3a where for the largest considered $L = 32$ μm, j_{sc} is approaching $j_{sc,bulk}$). Next, from the ideal diode equation $j = j_{sc} - j_0[\exp(eV/k_bT) - 1]$, we find that $V_{oc} \approx \log(j_{sc}/j_0)k_bT/e = \log[j_{sc,bulk}/(f \times j_{0,bulk})]k_bT/e = \log(1/f)k_bT/e + \log(j_{sc,bulk}/j_{0,bulk})k_bT/e$. Therefore, in this case, where nonradiative processes dominate the recombination and determine j_0, the V_{oc} could be increased compared to the bulk cell by $\Delta V_{oc} = \log(1/f)k_bT/e$. For example, for $f = 10\%$, an increase with $\Delta V_{oc} = 60$ mV could be obtained without sacrificing short-circuit current, leading to an efficiency beyond that reachable in the corresponding planar bulk cell. Thus, light concentration can lead to an enhanced open-circuit voltage and efficiency when nonradiative recombination limits the efficiency (notice that, as discussed above, the efficiency limit is lower in this case than in the case where the intrinsic radiative recombination limits the efficiency).

In contrast, in the case of a solar cell where radiative recombination limits the efficiency, light concentration in itself does not automatically increase the efficiency beyond that of a bulk cell. Since $A = e_{em}$, light concentration, that is, $A > f$, is accompanied by an enhanced emission per volume semiconductor material compared to the bulk cell, that is, $e_{em} > f$. That is, the light concentration is accompanied by the Purcell effect. Instead, to suppress j_0 below that in a bulk cell in order to lead to a higher efficiency limit, the emission must be suppressed for angles from which light is not incident from, as described in the main part of this paper.

CONCLUSIONS

We calculated the Shockley–Queisser efficiency limit for an InP nanowire array solar cell. This limit was obtained by considering both the absorption and emission of light in the nanowire array. The absorption of normally incident sunlight gives rise to the short-circuit current. The emission of photons is on the other hand an intrinsic process, which is exponentially enhanced by the voltage over the cell. These emitted photons originate from radiative recombination of electron–hole pairs. Thus, the emission puts a limit on the voltage under which photogenerated electron–hole pairs can contribute to the current that can be extracted from the solar cell. By considering these two optical processes, that is, the absorption and emission, we constructed the IV curve of the nanowire array solar cell. From this IV curve, we extracted the maximum power point, which yields the efficiency of the solar cell. The performance of the nanowire array solar cell was compared with a corresponding perfectly absorbing bulk InP solar cell when both cells were placed on an inactive high-refractive index substrate.

The nanowire array generated a lower short-circuit current than the bulk cell, showing for example for a nanowire length of 4 μm a maximum value of 96% of that obtainable in a bulk cell. However, the nanowire array emits at the same time fewer photons than the bulk cell, especially into the substrate. This weaker emission allows for a larger open-circuit voltage in the nanowire array solar cell. As an end result, nanowires longer than 4 μm can actually show, despite producing a lower short-circuit current, a higher efficiency limit than the bulk cell.

In this work, we considered an array of straight nanowires placed in a square pattern of 400 nm in period with air between and on top of the nanowires. We foresee future possibilities in affecting both the emission and absorption properties of the nanowire arrays, for example, by (i) varying the shape of the nanowires, (ii) varying the period of the array, (iii) coating the nanowires with a nonabsorbing dielectric shell, (iv) inserting a dielectric material between the nanowires, and (v) by introducing optical antireflection layers on top of the nanowire array. Such modification of the nanowire array could possibly further increase its efficiency limit.

AUTHOR INFORMATION

Corresponding Author

*E-mail: nicklas.anttu@ftf.lth.se.

Notes

The authors declare no competing financial interest.

ACKNOWLEDGMENTS

This work was supported by the Swedish Research Council (VR), the Swedish Foundation for Strategic Research (SSF), and the Nanometer Structure Consortium at Lund University (nmC@LU).

REFERENCES

(1) Wallentin, J.; Anttu, N.; Asoli, D.; Huffman, M.; Åberg, I.; Magnusson, M. H.; Siefer, G.; Fuss-Kailuweit, P.; Dimroth, F.; Witzigmann, B.; Xu, H. Q.; Samuelson, L.; Deppert, K.; Borgström, M. T. InP Nanowire Array Solar Cells Achieving 13.8% Efficiency by Exceeding the Ray Optics Limit. *Science* **2013**, *339*, 1057–1060.

(2) Goto, H.; Nosaki, K.; Tomioka, K.; Hara, S.; Hiruma, K.; Motohisa, J.; Fukui, T. Growth of Core-Shell InP Nanowires for Photovoltaic Application by Selective-Area Metal Organic Vapor Phase Epitaxy. *Appl. Phys. Express* **2009**, *2*, 035004.

DOI: 10.1021/ph5004835
ACS Photonics 2015, 2, 446–453

(3) Cui, Y.; Wang, J.; Plissard, S. R.; Cavalli, A.; Vu, T. T. T.; van Veldhoven, R. P. J.; Gao, L.; Trainor, M.; Verheijen, M. A.; Haverkort, J. E. M.; Bakkers, E. P. A. M. Efficiency Enhancement of InP Nanowire Solar Cells by Surface Cleaning. *Nano Lett.* **2013**, *13*, 4113−4117.
(4) Mariani, G.; Scofield, A. C.; Hung, C.-H.; Huffaker, D. L. GaAs Nanopillar-Array Solar Cells Employing In Situ Surface Passivation. *Nat. Commun.* **2013**, *4*, 1497.
(5) Yao, M. Q.; Huang, N. F.; Cong, S.; Chi, C. Y.; Seyedi, M. A.; Lin, Y. T.; Cao, Y.; Povinelli, M. L.; Dapkus, P. D.; Zhou, C. W. GaAs Nanowire Array Solar Cells with Axial p−i−n Junctions. *Nano Lett.* **2014**, *14*, 3293−3303.
(6) Kästner, G.; Gösele, U. Stress and Dislocations at Cross-sectional Heterojunctions in a Cylindrical Nanowire. *Philos. Mag.* **2004**, *84*, 3803−3824.
(7) Caroff, P.; Messing, M. E.; Borg, B. M.; Dick, K. A.; Deppert, K.; Wernersson, L. E. InSb Heterostructure Nanowires: MOVPE Growth under Extreme Lattice Mismatch. *Nanotechnology* **2009**, *20*, 495606.
(8) Wu, Y.; Fan, R.; Yang, P. Block-by-Block Growth of Single-Crystalline Si/SiGe Superlattice Nanowires. *Nano Lett.* **2002**, *2*, 83−86.
(9) Björk, M. T.; Ohlsson, B. J.; Sass, T.; Persson, A. I.; Thelander, C.; Magnusson, M. H.; Deppert, K.; Wallenberg, L. R.; Samuelson, L. One-Dimensional Steeplechase for Electrons Realized. *Nano Lett.* **2002**, *2*, 87−89.
(10) Gudiksen, M. S.; Lauhon, L. J.; Wang, J.; Smith, D. C.; Lieber, C. M. Growth of Nanowire Superlattice Structures for Nanoscale Photonics and Electronics. *Nature* **2002**, *415*, 617−620.
(11) Mårtensson, T.; Svensson, C. P. T.; Wacaser, B. A.; Larsson, M. W.; Seifert, W.; Deppert, K.; Gustafsson, A.; Wallenberg, L. R.; Samuelson, L. Epitaxial III−V Nanowires on Silicon. *Nano Lett.* **2004**, *4*, 1987−1990.
(12) Munshi, A. M.; Dheeraj, D. L.; Fauske, V. T.; Kim, D. C.; Huh, J.; Reinertsen, J. F.; Ahtapodov, L.; Lee, K. D.; Heidari, B.; van Helvoort, A. T. J.; Fimland, B. O.; Weman, H. Position-Controlled Uniform GaAs Nanowires on Silicon using Nanoimprint Lithography. *Nano Lett.* **2014**, *14*, 960−966.
(13) Muskens, O. L.; Rivas, J. G.; Algra, R. E.; Bakkers, E. P. A. M.; Lagendijk, A. Design of Light Scattering in Nanowire Materials for Photovoltaic Applications. *Nano Lett.* **2008**, *8*, 2638−2642.
(14) Wu, P. M.; Anttu, N.; Xu, H. Q.; Samuelson, L.; Pistol, M.-E. Colorful InAs Nanowire Arrays: from Strong to Weak Absorption with Geometrical Tuning. *Nano Lett.* **2012**, *12*, 1990−1995.
(15) Hu, L.; Chen, G. Analysis of Optical Absorption in Silicon Nanowire Arrays for Photovoltaic Applications. *Nano Lett.* **2007**, *7*, 3249−3252.
(16) LaPierre, R. R.; Chia, A. C. E.; Gibson, S. J.; Haapamaki, C. M.; Boulanger, J.; Yee, R.; Kuyanov, P.; Zhang, J.; Tajik, N.; Jewell, N.; Rahman, K. M. A. III−V Nanowire Photovoltaics: Review of Design for High Efficiency. *Phys. Status Solidi RRL* **2013**, *7*, 815−830.
(17) Krogstrup, P.; Jorgensen, H. I.; Heiss, M.; Demichel, O.; Holm, J. V.; Aagesen, M.; Nygard, J.; Fontcuberta i Morral, A. Single-Nanowire Solar Cells Beyond the Shockley−Queisser Limit. *Nat. Photonics* **2013**, *7*, 306−310.
(18) Anttu, N.; Xu, H. Q. Efficient Light Management in Vertical Nanowire Arrays for Photovoltaics. *Opt. Express* **2013**, *21*, A558−A575.
(19) Anttu, N. Geometrical Optics, Electrostatics, and Nanophotonic Resonances in Absorbing Nanowire Arrays. *Opt. Lett.* **2013**, *38*, 730−732.
(20) Dhindsa, N.; Chia, A.; Boulanger, J.; Khodadad, I.; LaPierre, R.; Saini, S. S. Highly Ordered Vertical GaAs Nanowire Arrays with Dry Etching and Their Optical Properties. *Nanotechnology* **2014**, *25*, 305303.
(21) Zhang, J. P.; Dhindsa, N.; Chia, A.; Boulanger, J.; Khodadad, I.; Saini, S.; LaPierre, R. Multi-Spectral Optical Absorption in Substrate-Free Nanowire Arrays. *Appl. Phys. Lett.* **2014**, *105*, 123113.
(22) Seo, K.; Wober, M.; Steinvurzel, P.; Schonbrun, E.; Dan, Y. P.; Ellenbogen, T.; Crozier, K. B. Multicolored Vertical Silicon Nanowires. *Nano Lett.* **2011**, *11*, 1851−1856.
(23) Wang, B. M.; Leu, P. W. Tunable and Selective Resonant Absorption in Vertical Nanowires. *Opt. Lett.* **2012**, *37*, 3756−3758.
(24) Anttu, N.; Xu, H. Q. Coupling of Light into Nanowire Arrays and Subsequent Absorption. *J. Nanosci. Nanotechnol.* **2010**, *10*, 7183−7187.
(25) Anttu, N.; Abrand, A.; Asoli, D.; Heurlin, M.; Åberg, I.; Samuelson, L.; Borgström, M. Absorption of Light in InP Nanowire Arrays. *Nano Res.* **2014**, *7*, 816−823.
(26) Huang, N. F.; Lin, C. X.; Povinelli, M. L. Broadband Absorption of Semiconductor Nanowire Arrays for Photovoltaic Applications. *J. Opt.* **2012**, *14*, 024004.
(27) Kupec, J.; Stoop, R. L.; Witzigmann, B. Light Absorption and Emission in Nanowire Array Solar Cells. *Opt. Express* **2010**, *18*, 27589−27605.
(28) Shockley, W.; Queisser, H. J. Detailed Balance Limit of Efficiency of P−N Junction Solar Cells. *J. Appl. Phys.* **1961**, *32*, 510−519.
(29) Miller, O. D.; Yablonovitch, E.; Kurtz, S. R. Strong Internal and External Luminescence as Solar Cells Approach the Shockley−Queisser Limit. *IEEE J. Photovolt.* **2012**, *2*, 303−311.
(30) Yablonovitch, E. Inhibited Spontaneous Emission in Solid-State Physics and Electronics. *Phys. Rev. Lett.* **1987**, *58*, 2059−2062.
(31) Sandhu, S.; Yu, Z.; Fan, S. Detailed Balance Analysis of Nanophotonic Solar Cells. *Opt. Express* **2013**, *21*, 1209−1217.
(32) Paniagua-Dominguez, R.; Grzela, G.; Rivas, J. G.; Sanchez-Gil, J. A. Enhanced and Directional Emission of Semiconductor Nanowires Tailored Through Leaky/Guided Modes. *Nanoscale* **2013**, *5*, 10582−10590.
(33) Grzela, G.; Paniagua-Dominguez, R.; Barten, T.; Fontana, Y.; Sanchez-Gil, J. A.; Rivas, J. G. Nanowire Antenna Emission. *Nano Lett.* **2012**, *12*, 5481−5486.
(34) Saleh, B. E. A.; Teich, M. C. *Fundamentals of Photonics*; Wiley: NJ, 2007.
(35) Air Mass 1.5 Spectra, American Society for Testing and Materials, http://rredc.nrel.gov/solar/spectra/am1.5/.
(36) LaPierre, R. R. Numerical Model of Current-Voltage Characteristics and Efficiency of GaAs Nanowire Solar Cells. *J. Appl. Phys.* **2011**, *109*, 034311.
(37) LaPierre, R. R. Theoretical Conversion Efficiency of a Two-Junction III−V Nanowire on Si Solar Cell. *J. Appl. Phys.* **2011**, *110*, 014310.
(38) Huang, N. F.; Lin, C. X.; Povinelli, M. L. Limiting Efficiencies of Tandem Solar Cells Consisting of III−V Nanowire Arrays on Silicon. *J. Appl. Phys.* **2012**, *112*, 064321.
(39) Bu, S. J.; Li, X. H.; Wen, L.; Zeng, X. S.; Zhao, Y. F.; Wang, W. B.; Wang, Y. Q. Optical and Electrical Simulations of Two-junction III−V Nanowires on Si Solar Cell. *Appl. Phys. Lett.* **2013**, *102*, 031106.
(40) Wen, L.; Li, X. H.; Zhao, Z. F.; Bu, S. J.; Zeng, X. S.; Huang, J. H.; Wang, Y. Q. Theoretical Consideration of III−V Nanowire/Si Triple-Junction Solar Cells. *Nanotechnology* **2012**, *23*, 505202.
(41) We note that a similar assumption of perfect absorption has been used previously for the analysis of nanowire array solar cells.[38] However, as shown below, the emission properties of a nanowire array solar cell differ strongly from those of a perfectly absorbing bulk cell, modifying the reverse bias saturation current density j_0 and, hence, also the open-circuit voltage and the efficiency.
(42) Anttu, N.; Xu, H. Q. Scattering Matrix Method for Optical Excitation of Surface Plasmons in Metal Films with Periodic Arrays of Subwavelength Holes. *Phys. Rev. B* **2011**, *83*, 165431.
(43) Glembocki, O. J.; Piller, H. Indium Phosphide (InP). In *Handbook of Optical Constants of Solids*; Palik, E. D., Ed.; Academic: Burlington, 1997; pp 503−516.
(44) Munday, J. N. The Effect of Photonic Bandgap Materials on the Shockley−Queisser Limit. *J. Appl. Phys.* **2012**, *112*, 064501.
(45) Note that we assume throughout this work, as is conventionally done,[28,31] that the emission is zero for $\lambda > \lambda_{bg}$. That is, we make an energy cutoff for photons at an energy of E_{bg}. We show in Figure 5 also the modeled emission for $\lambda > \lambda_{bg}$, and we find that approximately one-third of the emitted photons could originate from this region of $\lambda >$

DOI: 10.1021/ph5004835
ACS Photonics 2015, 2, 446−453

λ_{bg}. Such an increase of F_{c0} by a factor of 1.5 would lower V_{oc} by 10 mV through eq 4, that is, approximately by 1%. Notice that by relaxing the energy cutoff when calculating j_{sc} in eq 3 to allow for absorption of photons with $\lambda > \lambda_{bg}$ would on the other hand increase j_{sc} by approximately 1%. Thus, we do not expect that the energy cutoff at E_{bg} has a considerable effect on the efficiency limit derived here.

(46) Kosten, E. D.; Atwater, J. H.; Parsons, J.; Polman, A.; Atwater, H. A. Highly Efficient GaAs Solar Cells by Limiting Light Emission Angle. *Light: Sci. Appl.* **2013**, *2*, e45.

DOI: 10.1021/ph5004835
ACS Photonics 2015, 2, 446−453